The origin of the . 1.7 Ga gabbroic intrusion in the Hekou area, SW China: constraints from SIMS U–Pb zircon geochronology and elemental and Nd isotopic geochemistry

WEI-GUANG ZHU*, ZHONG-JIE BAI, HONG ZHONG, XIAN-TAO YE
& HONG-PENG FAN

State Key Laboratory of Ore Deposit Geochemistry, Institute of Geochemistry, Chinese Academy of Sciences, 99 West Lincheng Road, Guiyang 550081, China

Abstract – The late Palaeoproterozoic to early Mesoproterozoic igneous rocks of southwestern China are characterized by a number of mafic intrusions and dykes. However, the origin and tectonic implications of these mafic intrusions and dykes remain unclear. The Hekou mafic intrusion, intruding into the Hekou Group in the Hekou area, SW China, is the biggest and most representative one. The intrusion is mainly composed of coarse-grained in the central zone (CZ) and medium- to fine-grained gabbroic rocks in the outer zone (OZ). Cameca secondary ion mass spectroscopy (SIMS) U–Pb zircon ages, and geochemical and Nd isotopic results for the intrusion are reported in this paper. SIMS U–Pb zircon ages indicate that the gabbroic rocks from the CZ and OZ were emplaced at 1735 ± 6.5 Ma and 1736 ± 4.0 Ma, respectively. This suggests that the Hekou intrusion originated from . 1.7 Ga mafic magmatism in the southwestern Yangtze Block. The coarse-grained rocks in the CZ of the intrusion show fairly homogeneous major- and trace-element compositions. In contrast, the medium- to fine-grained rocks from the OZ display slightly evolved compositions, with relatively lower Mg nos, MgO, Al_2O_3, Cr and Ni contents, and higher SiO_2, CaO and Zr concentrations than those of the rocks from the CZ. Although the gabbroic rocks of the intrusion have low total rare earth element (REE) contents (REE = 29.3–40.2 ppm) with slightly light REE (LREE)-enriched and heavy REE (HREE)-depleted patterns, they exhibit distinct trace-element and Nd isotopic features. The rocks from the CZ are characterized by slightly LREE-enriched and 'convex upwards' incompatible trace-element patterns with significant Th depletion and insignificant Nb and Ta depletion relative to La. However, the rocks from the OZ have relatively flatter REE patterns than those of the rocks from the CZ. In addition, the rocks from the OZ are slightly enriched in Th and depleted in Nb and Ta relative to La. The $\varepsilon_{Nd}(T)$ values of the CZ and the OZ rocks are +0.70 to +2.3 and −0.30 to +0.24, respectively. The parental magma for the Hekou gabbroic intrusion exhibits affinity with a subalkaline basaltic magma, which was possibly generated by relatively high degrees of partial melting of a slightly depleted asthenospheric mantle source. Their geochemical and isotopic variations were due to slight crystal fractionation with varying degrees of crustal contamination. The Hekou intrusion was therefore supposed to form in an anorogenic extensional environment. It is further suggested that . 1.7 Ga is an important onset timing of widespread anorogenic magmatism in the southwestern Yangtze Block. We interpret the late Palaeoproterozoic gabbroic intrusion to represent anorogenic mafic magmatism, which was most likely related to the break-up of the Columbia supercontinent.

Keywords: late Palaeoproterozoic, gabbroic intrusion, zircon geochronology, anorogenic magmatism, southwestern Yangtze Block, Columbia supercontinent.

1. Introduction

The South China Craton, including the Yangtze Block to the northwest and the Cathaysia Block to the southeast (present coordinates), was presumably the central part of the Precambrian supercontinent Rodinia (Fig. 1a) (Li, Zhang & Powell, 1995). Apart from the Kongling Complex, there have been three other major rock units previously reported from the Yangtze Block, including some volcanic and meta-volcanic rocks of late Palaeoproterozoic to Mesoproterozoic age. The . 1.75–1.66 Ga Dahongshan Group (marked '2' in Fig. 1a) consists of meta-volcaniclastic rocks,

meta-basalts, meta-siliciclastic rocks and marble (e.g. Greentree & Li, 2008; Zhao t . 2010). The Tianli schists (marked '3' in Fig. 1a) represent a clastic sedimentary succession, probably formed on the southern continental shelf of the Yangtze Block between . 1530 Ma and 1042 Ma (Li t . 2007). The Kunyang–Huili groups (marked '4' in Fig. 1a) consist of a sequence of greenschist-facies meta-sedimentary and meta-volcanic rocks that probably developed between 1.8 Ga and 1.0 Ga (Greentree t . 2006; Greentree & Li, 2008; Zhao t . 2010).

The Yangtze Block played an important role in the reconstruction of the Rodinia supercontinent (e.g. Li, Zhang & Powell, 1995; Li t . 2002, 2008), but little is known as to whether or not it was also a component
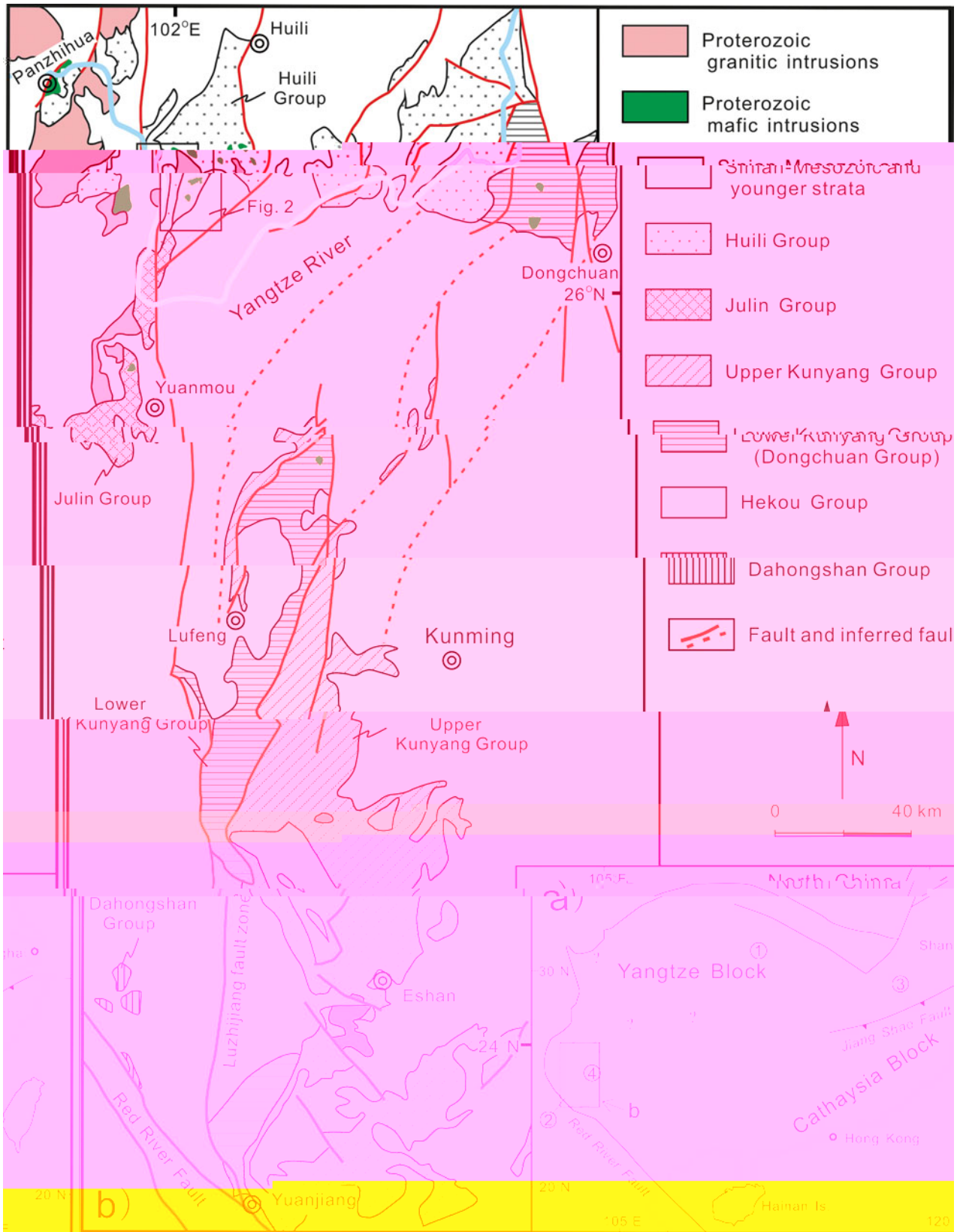
*Author for correspondence: zhuweiguang@vip.gyig.ac.cn

Figure 1. (Colour online) (a) Simplified tectonic map showing the study area in relation to South China's major tectonic units (Li *t* .
2007). Numbers 1–4 indicate the Kongling Complex, the Dahongshan Group, the Tianli schists and the Kunyang–Dongchuan groups,
respectively; (b) geological map of the late Palaeo- to Mesoproterozoic strata and Proterozoic intrusions in the Kangdian region, SW
China (modified from Wu *t* . 1990; Zhao & Zhou, 2011).

of the Palaeo- to Mesoproterozoic supercontinent called Nuna (Hoffman, 1989, 1997; Evans & Mitchell, 2011; Zhang *t* . 2012) or Columbia (Rogers & Santosh, 2002; Zhao *t* . 2002 ; Hou *t* . 2008 ; Meert, 2012; we will use this name in the remainder of this paper for the late Palaeo- to Mesoproterozoic supercontinent). Nonetheless, 2.03–1.97 Ga granulites and 1.85 Ga A-type granites and mafic dykes have been identified in the northern part of the Yangtze Block (the Kongling Complex; '1' in Fig. 1a) (Zhang *t* . 2006 ; Sun *t* . 2008; Wu *t* . 2008; Xiong *t* . 2009; Peng *t* . 2009, 2012), which coincide with the age of the Columbia supercontinent assembly (Hoffman, 1989, 1997), and may therefore be genetically linked to the evolution of the supercontinent. Yao, Shu & Santosh (2011) presented evidence from detrital zircon U–Pb geochronology, Hf isotopes and geochemistry from the Cathaysia Block (Fig. 1a) with clear age peaks at 1930–1520 Ma, which they correlated with the Columbia supercontinent. In addition, a number of studies have documented the late Palaeoproterozoic to early Mesoproterozoic igneous rocks in the southwestern Yangtze Block in recent years. The presence of late Palaeoproterozoic to early Mesoproterozoic (1.7–1.5 Ga) mafic magmatism in the southwestern Yangtze Block is contemporaneous with the break-up of the Columbia supercontinent, and provides further evidence to support the idea that the Yangtze Block was likely a part of the Columbia supercontinent (Zhao *t* . 2010, 2013; Fan *t* . 2013). Meanwhile, the Yinmin Formation of the Lower Kunyang Group in the southwestern Yangtze Block contains zircons of ages dominantly from late Archaean to Palaeoproterozoic (2.8–2.7 Ga, 2.5–2.3 Ga and . 1.85 Ga). The Heishantou Formation of the Upper Kunyang Group has two major age populations, i.e. 1.8–1.6 Ga and . 1.0 Ga. The presence of abundant . 1.85 Ga zircons also suggests that the Yangtze Block was probably a part of the Columbia supercontinent during Palaeoproterozoic time (Wang *t* . 2012).

In recent years, many intrusive igneous rocks in the southwestern Yangtze Block have been gradually identified in age as late Palaeoproterozoic to early Mesoproterozoic, although these intrusive igneous rocks in the Kangdian region are sparse and on a small scale. For example, a number of mafic intrusions and dykes intruded into the Dahongshan Group, Lower Kunyang Group (also called the Dongchuan Group; we will use the name Lower Kunyang Group in the remainder of the paper), Hekou Group and Huili Group in the Kangdian region (Zhao *t* . 2010, 2013; Guan *t* . 2011; Zhao & Zhou, 2011; Fan *t* . 2013). A dolerite dyke cutting the Dahongshan Group has a laser ablation inductively couple plasma mass spectrometry (LA-ICP-MS) U–Pb zircon age of 1659 ± 16 Ma (Zhao & Zhou, 2011). The other dolerite dykes that cut the Yinmin Formation of the Lower Kunyang Group have LA-ICP-MS and a secondary ion mass spectroscopy (SIMS) U–Pb zircon ages of 1690 ± 32 Ma (Zhao *t* . 2010) and 1701 ± 28 Ma (Zhao *t* . 2013), respectively.

In addition, the Zhuqing Fe–Ti–V oxide ore-bearing mafic intrusions that intruded into the Huili Group were dated at 1494 ± 6 Ma (zircon U–Pb), 1486 ± 3 Ma and 1490 ± 4 Ma (baddeleyite U–Pb), respectively (Fan *t* . 2013). However, owing to the lack of more systematic geochemical and isotopic data, the origin and tectonic implications of these mafic dykes and intrusions remain unclear. Thus, further studies on the timing and tectonic setting of these mafic dykes and intrusions are needed, which will play an important role in elucidating the late Palaeoproterozoic to early Mesoproterozoic tectonic evolution of the southwestern Yangtze Block.

There are numerous mafic intrusions that intruded the Hekou Group in the Hekou area, SW Huili County (D. F. He, unpub. Ph.D. thesis, Graduate School of the Chinese Academy of Sciences, 2009; Zhou *t* . 2009; Guan *t* . 2011; Chen & Zhou, 2012; Chen, Zhou & Zhao, 2013). Recent studies have focused on the ages of these intrusions. The . 1.7 Ga dolerite and gabbroic intrusions that intruded into the Hekou Group were recently identified in the Hekou area (Guan *t* . 2011; Chen, Zhou & Zhao, 2013). However, Guan *t* . (2011) reported a SHRIMP zircon age of 1710 ± 8 Ma for a dolerite intrusion that intruded into the Hekou Group, which is very different from the whole-rock Sm–Nd isochron age of . 850 Ma for some gabbroic and dolerite intrusions in this area (Zhou *t* . 2009). In addition, the petrogenesis of the mafic intrusions is not well understood in this area. Thus, systematic geochronological, elemental and Nd isotopic investigations on these rocks are further required to elucidate the origin and tectonic implications of these mafic intrusions.

In this paper, we report precise Cameca SIMS U–Pb zircon ages, and geochemical and Nd isotopic data for the biggest and most representative Hekou gabbroic intrusion in the Hekou area with the aim to (1) date the crystallization age for the gabbroic intrusion; (2) constrain the origin and petrogenesis of the intrusion; and (3) shed new light on the late Palaeoproterozoic tectonic evolution in the southwestern Yangtze Block. Our new results confirm that the gabbroic intrusion emplaced at . 1.7 Ga in the Hekou area was derived from a slightly depleted mantle source and formed in an intracontinental rift, most likely related to the break-up of the Columbia supercontinent.

2. Geological background and petrography

The South China Craton consists of two major Precambrian blocks: the Yangtze Block and the Cathaysia Block (present coordinates) (Fig. 1a; Li *t* . 2007). The oldest rocks exposed in the Yangtze Block are the Kongling complex (marked '1' in Fig. 1a) containing magmatic and metamorphic rocks as old as 3.3 Ga (Zhang *t* . 2006 ; Gao *t* . 2011). Zheng *t* . (2006) suggested a wide distribution of Archaean rocks in the unexposed basement of the Yangtze Block based on U–Pb and Hf isotopic data from zircon xenocrysts in Palaeozoic lamproites. Zhao *t* . (2010) and Wang

t . (2012) reached the same conclusion based on detrital zircon analyses of Palaeo- to Neoproterozoic sedimentary rocks in the southwestern Yangtze Block. These recent studies have proposed that the Archaean to Palaeoproterozoic basement is probably more widespread in the Yangtze Block than previously thought (Zheng *t* . 2006; Zhang *t* . 2006 , ; Wang *t* . 2010, 2012).

The Kangdian area (Fig. 1b) is located near the southwestern margin of the Yangtze Block (Fig. 1a). The oldest supracrustal rocks in this area are the late Palaeo- to Mesoproterozoic meta-volcanic and meta-sedimentary rocks, termed the Dahongshan Group (Greentree & Li, 2008), the Lower Kunyang Group (Dongchuan Group; Zhao *t* . 2010), the Hekou Group (Wu *t* . 1990; D. F. He, unpub. Ph.D. thesis, Graduate School of the Chinese Academy of Sciences, 2009; Zhao & Zhou, 2011), the Huili Group (Yin, Sun & Zhang, 2011) and the Kunyang Group (Yin, Sun & Zhang, 2011), which occur along the Luzhijiang fault and a series of related NNE-trending faults (Fig. 1b). They consist of meta-sedimentary rocks interbedded with felsic and mafic meta-volcanic rocks (Li *t* . 2002, 2006; Greentree *t* . 2006; Greentree & Li, 2008; Zhao *t* . 2010). These late Palaeo- to Mesoproterozoic rocks are overlain by a thick sequence (maximum > 9 km) of Neoproterozoic (850–540 Ma) to Permian strata consisting of clastic, carbonate and volcanic rocks (Cong, 1988; SBGMR, 1991).

The ages of the Precambrian units in the Kangdian region had been poorly constrained (see review by Wu *t* . 1990) until the availability of precise U–Pb zircon ages in recent years. The Dahongshan Fe–Cu ore deposit is hosted in the Dahongshan Group (Zhao & Zhou, 2011). Meta-volcanic units in the Dahongshan Group have been dated at 1675 ± 8 Ma and 1681 ± 13 Ma by SHRIMP U–Pb zircon (Greentree & Li, 2008) and LA-ICP-MS U–Pb zircon (Zhao & Zhou, 2011) methods, respectively.

The Kunyang Group in the southern part of the study region (Fig. 1b) was divided into the Upper and Lower Kunyang groups (e.g. Zhao *t* . 2010; Zhao & Zhou, 2011; Yin, Sun & Zhang, 2011). From the base upwards, the Lower Kunyang Group (Zhao *t* . 2010; Zhao & Zhou, 2011; Yin, Sun & Zhang, 2011) includes the Yinmin, Luoxue, E'touchang and Luzhijiang formations, whereas the Upper Kunyang Group consists of the Dayingpan, Heishantou, Dalongkou and Meidang formations. Several 'Dongchuan-type' Fe–Cu ore deposits are hosted in the Lower Kunyang Group (Zhao *t* . 2010, 2013; Zhao & Zhou, 2011). Detrital zircons from the Lower Kunyang Group yielded the youngest age of . 1.78 Ga, and a tuff sample from the same group has a U–Pb zircon age of 1742 ± 13 Ma (Zhao *t* . 2010). Sun *t* . (2009) recently reported a SHRIMP zircon age of 1503 ± 17 Ma for a tuff sample from the E'touchang Formation in the Lower Kunyang Group. Thus, the Lower Kunyang Group likely formed between . 1.7 Ga and . 1.5 Ga. Zhao *t* . (2010) hence interpreted the Lower Kunyang (Dongchuan)

and Dahongshan groups as stratigraphically correlatable units (Fig. 1b). In addition, a carbonaceous shale sample of the Dayingpan Formation from the Upper Kunyang Group yielded a whole-rock Pb–Pb isochron age of 1258 ± 70 Ma (Chang *t* . 1997). A tuff layer in the Heishantou Formation of the Upper Kunyang Group has been dated at 995 ± 15 Ma and 1032
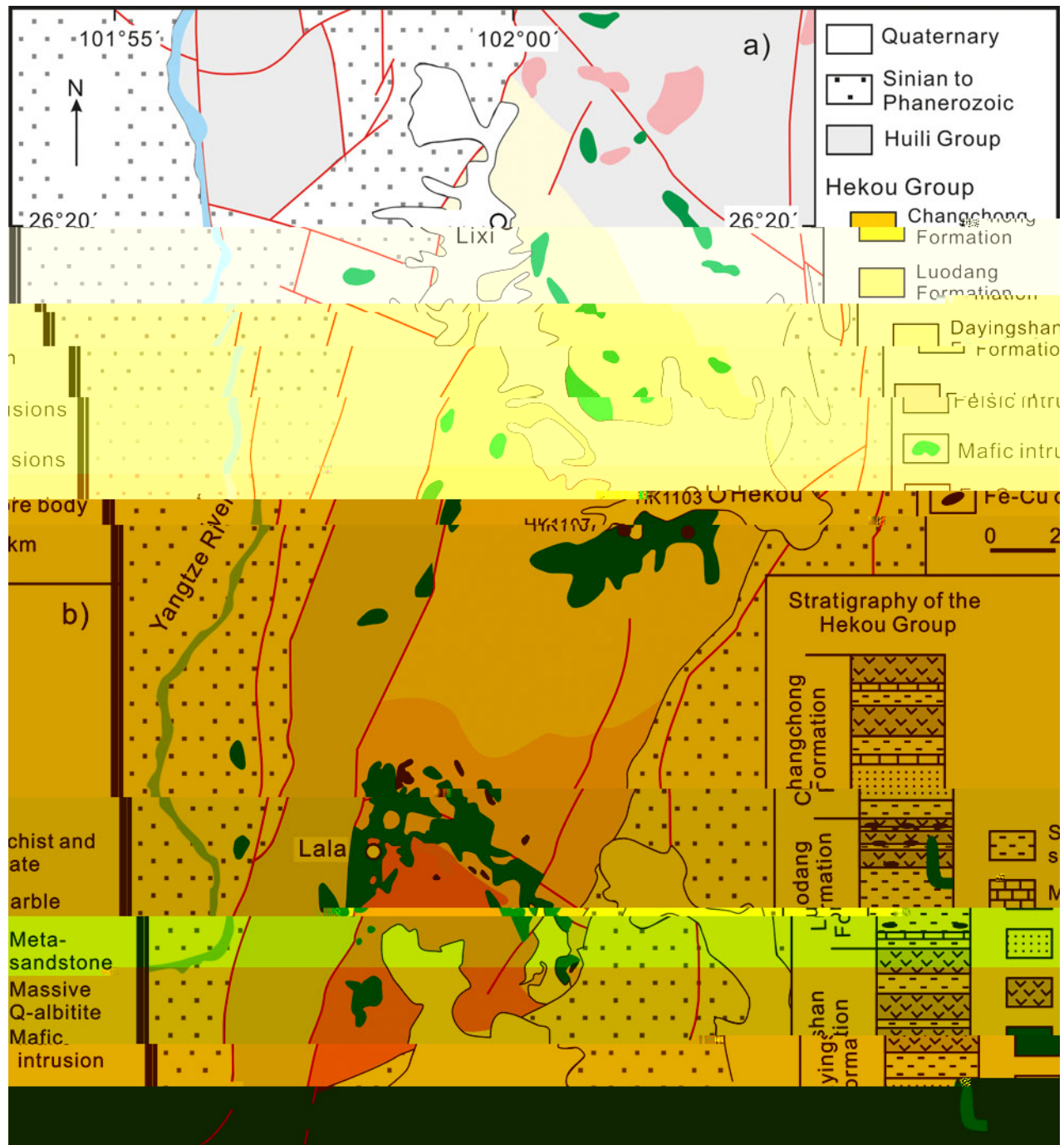
Figure 2. (Colour online) (a) A simplified geologic map of the Hekou area, Sichuan Province, SW China; (b) a simplified stratigraphic column of the Hekou Group. Modified from the Chinese Huili 1:200 000 geological map (SBG, 1967).

~30–45°. The intrusion is the biggest mafic intrusion in the Hekou area and is up to 4–5 km long with a thickness between 1 and 2 km, covering an area of about 6 km² (Fig. 2a). These rocks are dark-grey to black, fine to coarse grained, with massive and subhedral granular and ophitic textures. The coarse-grained gabbroic rocks are in the central zone (CZ) of the intrusion, and are moderately to strongly altered to chlorite, actinolite and albite. However, the medium- to fine-grained gabbroic rocks are usually observed in the outer zone (OZ) of the intrusion, and are relatively fresh to slightly altered. These rocks mainly consist of plagioclase (50–55 vol. % by volume) and clinopyroxene (40–45 vol. %), and minor subordinate orthopyroxene, Fe–Ti oxides and apatite. Clinopyroxenes in the gabbros from the OZ commonly exhibit a medium- to fine-grained texture. Electron microprobe analyses indicate clinopyroxenes from the gabbros are $Wo_{38-49}En_{34-46}Fs_{11-22}$, mostly belonging to augite (online Supplementary Material available at http://journals.cambridge.org/geo).

3. Sampling and analytical methods

Nineteen samples were collected from the CZ (samples HK1101 to HK1103) and the OZ (samples HK1104 to

HK1211) of the gabbroic intrusion in the Hekou area (Fig. 2a, b).

Zircons from samples HK1103 and HK1107 were separated using conventional heavy liquid and magnetic techniques, then by handpicking under binocular microscopes. They were mounted in an epoxy resin disc, and polished and coated with gold film. Zircons were documented with transmitted and reflected light micrographs as well as cathodoluminescence (CL) images to reveal their external and internal structures. U–Pb zircon dating was conducted using a Cameca IMS 1280 ion microprobe (SIMS) at the Institute of Geology and Geophysics, the Chinese Academy of Sciences (CAS) in Beijing. Details of the analytical procedures for U–Pb zircon dating can be found in Li *t . (2009, 2010)*. Oxygen flooding that introduces oxygen into the sample chamber was used during the analyses, which not only enhances Pb$^+$ ion yield by a factor of 2 and 7 for zircon and baddeleyite (Li *t . 2009*), respectively, but also depresses the U–Pb orientation effect (Wingate & Compston, 2000) down to ~2 % (Li *t . 2010*). The uncertainties in ages are cited as 1σ, and the weighted mean ages are quoted at the 95 % confidence interval (2σ). The SIMS U–Pb zircon ages are presented in Table 1.

Chemical compositions of clinopyroxenes from the gabbroic intrusion were determined by wavelength-dispersion X-ray emission spectrometry using an EPMA-1600 electron microprobe at the State Key Laboratory of Ore Deposit Geochemistry (SKLODG), Institute of Geochemistry, Chinese Academy of Sciences (IGCAS). Major-element compositions of whole rocks were determined using X–ray fluorescence spectrometers (XRF) at the State Key Laboratory of Isotope Geochemistry, Guangzhou Institute of Geochemistry of the CAS. The analytical precision was better than 5 %. Trace elements in whole rocks were analysed using a Perkin-Elmer Sciex ELAN DRC–e ICP-MS at the SKLODG, IGCAS. The powdered samples (50 mg) were dissolved with HF + HNO$_3$ mixture in high-pressure Teflon bombs at ~190 °C for 48 hours (Qi, Hu & Gregoire, 2000). Rh was used as an internal standard to monitor signal drift during measurement. The international standards GBPG-1, OU-6 and the Chinese National standards GSR-1 and GSR-3, were used for analytical quality control. The analytical precision is generally better than 10 % for trace elements.

Samples for Nd isotopic analyses were dissolved in an acidic mixture of HF, HNO$_3$ and HClO$_4$ in Teflon bombs. Sm and Nd were separated by conventional cation-exchange techniques at the SKLODG. The Nd isotopic measurements were performed on a multicollector ICP-MS (MC-ICP-MS) at the Key Laboratory of Orogenic Belts and Crustal Evolution, School of Earth and Space Sciences, Peking University. The mass fractionation corrections for Nd isotopic ratios are based on ^{146}Nd/^{144}Nd = 0.7219. The ^{143}Nd/^{144}Nd ratios of the JNDI-1 Nd standard solution and the USGS standard rock BCR-2 were determined to be 0.512119 ± 14 (2σ) and 0.512629 ± 16 (2σ), respectively.
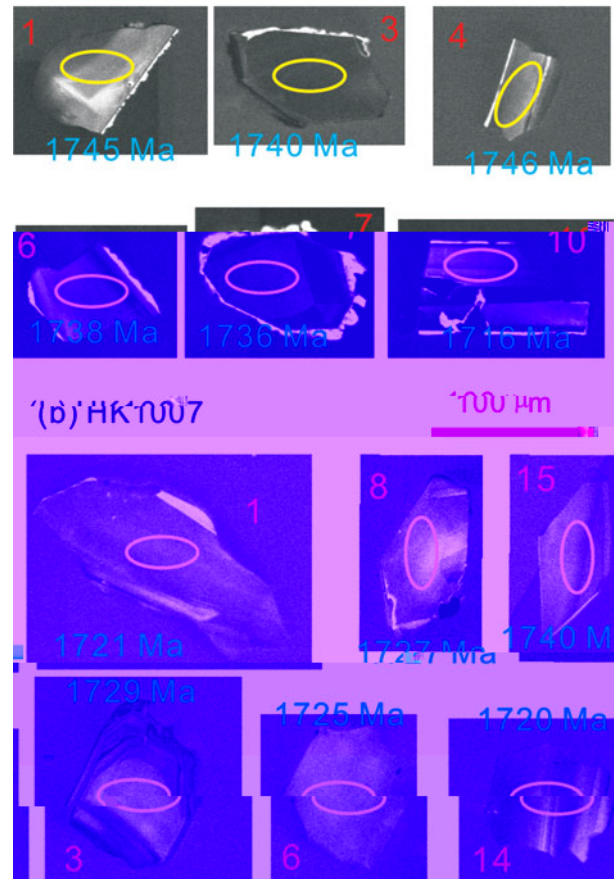

Figure 3. (Colour online) Representative CL images of zircons from (a) sample HK1003 from the CZ; and (b) sample HK1007 from the OZ of the gabbroic rocks from the Hekou intrusion.

4. Results

4.a. U–Pb zircon geochronology

4. .1.   1103 (2 °1 ′ 12. ″ , 102°01′ 04. ″)

Zircons extracted from sample HK1103 in the CZ are mostly clear and up to 50–100 μm in length with length to width ratios between 1:1 and 1.5:1. Most zircons are simple prismatic crystals without obvious zoning under CL (Fig. 3a). Fourteen analyses were conducted on 14 zircons. Uranium and thorium concentrations are variable, with U = 213–1263 ppm, Th = 83–2879 ppm and Th/U = 0.31–3.79 (Table 1). Most analyses yielded near concordant ages, while four grains are obviously discordant owing to the loss of radiogenic lead. All 14 analyses give consistent ^{207}Pb/^{206}Pb ratios within errors, yielding a weighted average ^{207}Pb/^{206}Pb age of 1736 ± 5.0 Ma (95 % confidence interval, MSWD = 1.5). In addition, all these analyses yield a discordia line with an upper intercept age of 1735 ± 6.5 Ma (MSWD = 4.9) (Fig. 4a).

4. .2.   110 (2 °1 ′ 25.0″ , 102°00′ 2 . ″)

Zircons from sample HK1107 from the OZ are mostly clear, euhedral prismatic grains without obvious zoning

Table 1. Cameca SIMS U–Pb zircon isotopic analyses for the gabbroic rocks from the Hekou intrusion, SW China

| Spot | U (ppm) | Th (ppm) | Th/U | $^{206}Pb/^{204}Pb$ measured | f_{206} (%) | Isotopic ratio | | | | | | Age/Ma | |
						$^{207}Pb^*/^{206}Pb^*$	$\pm 1\sigma$ (%)	$^{207}Pb^*/^{235}U$	$\pm 1\sigma$ (%)	$^{206}Pb^*/^{238}U$	$\pm 1\sigma$ (%)	$^{206}Pb^*/^{238}U \pm 1\sigma$	$^{207}Pb^*/^{206}Pb^* \pm 1\sigma$
HK1103 (26° 16′ 12.7″ N, 102° 01′ 04.6″ E)													
1	213	462	2.169	55680	0.03	0.10679	0.70	4.51721	1.67	0.3068	1.52	1725 ± 23	1745 ± 13
2	423	419	0.991	29413	0.06	0.10685	0.40	4.28050	1.56	0.2906	1.50	1644 ± 22	1746 ± 7
3	1263	820	0.649	34369	0.05	0.10645	0.29	4.54819	1.53	0.3099	1.50	1740 ± 23	1740 ± 5
4	761	2879	3.786	135897	0.01	0.10682	0.31	4.47788	1.54	0.3040	1.51	1711 ± 23	1746 ± 6
5	819	893	1.091	31703	0.06	0.10555	0.30	4.64353	1.53	0.3191	1.50	1785 ± 23	1724 ± 5
6	387	999	2.579	97461	0.02	0.10638	0.41	4.53021	1.56	0.3089	1.50	1735 ± 23	1738 ± 7
7	651	849	1.304	8633	0.22	0.10622	0.35	4.43688	1.54	0.3029	1.50	1706 ± 23	1736 ± 6
8	903	1133	1.254	17637	0.11	0.10601	0.42	4.45005	1.85	0.3045	1.80	1713 ± 27	1732 ± 8
9	545	1219	2.238	17646	0.11	0.10676	0.36	4.53833	1.55	0.3083	1.51	1732 ± 23	1745 ± 6
10	264	83	0.313	14126	0.13	0.10512	0.57	4.41465	1.61	0.3046	1.50	1714 ± 23	1716 ± 10
11	702	701	0.997	74992	0.02	0.10607	0.41	4.46068	1.56	0.3050	1.50	1716 ± 23	1733 ± 8
12	376	128	0.341	378261	0.00	0.10580	0.43	4.45464	1.56	0.3054	1.50	1718 ± 23	1728 ± 8
13	234	363	1.553	7342	0.25	0.10556	0.59	4.29977	1.63	0.2954	1.52	1669 ± 22	1724 ± 11
14	624	526	0.843	37683	0.05	0.10637	0.60	4.26915	1.62	0.2911	1.50	1647 ± 22	1738 ± 11
HK1107 (26° 16′ 25.0″ N, 102° 00′ 26.6″ E)													
1	1092	1360	1.246	383479	0.00	0.10537	0.25	4.49558	1.53	0.3094	1.51	1738 ± 23	1721 ± 5
2	745	823	1.105	460231	0.00	0.10614	0.52	4.54199	1.60	0.3104	1.51	1742 ± 23	1734 ± 9
3	531	583	1.097	-	0.00	0.10582	0.36	4.47960	1.54	0.3070	1.50	1726 ± 23	1729 ± 7
4	500	478	0.958	99383	0.02	0.10546	0.93	4.58524	1.76	0.3153	1.50	1767 ± 23	1722 ± 17
5	990	1369	1.383	243753	0.01	0.10595	0.50	4.50988	1.58	0.3087	1.50	1734 ± 23	1731 ± 9
6	567	649	1.144	174437	0.01	0.10559	0.39	4.51745	1.57	0.3103	1.52	1742 ± 23	1725 ± 7
7	509	642	1.261	355791	0.01	0.10592	0.70	4.52209	1.67	0.3097	1.51	1739 ± 23	1730 ± 13
8	364	388	1.067	-	0.00	0.10574	0.65	4.48167	1.64	0.3074	1.51	1728 ± 23	1727 ± 12
9	1533	2527	1.648	62416	0.03	0.10588	0.23	4.60162	1.52	0.3152	1.50	1766 ± 23	1730 ± 4
10	513	552	1.076	431146	0.00	0.10636	0.47	4.57161	1.57	0.3117	1.50	1749 ± 23	1738 ± 9
11	752	915	1.217	225562	0.01	0.10627	0.58	4.54545	1.63	0.3102	1.53	1742 ± 23	1736 ± 11
12	533	587	1.101	444455	0.00	0.10568	0.38	4.54519	1.55	0.3119	1.50	1750 ± 23	1726 ± 7
13	1228	1827	1.489	114192	0.02	0.10568	0.28	4.60487	1.54	0.3160	1.51	1770 ± 23	1726 ± 5
14	733	1084	1.478	7367	0.25	0.10531	0.49	4.60418	1.71	0.3171	1.64	1775 ± 25	1720 ± 9
15	606	681	1.125	1115	1.68	0.10650	0.97	4.53159	1.80	0.3086	1.52	1734 ± 23	1740 ± 18
16	526	535	1.017	267107	0.01	0.10616	0.39	4.53277	1.55	0.3097	1.50	1739 ± 23	1735 ± 7
17	302	530	1.751	2517	0.74	0.10656	1.72	4.57184	2.28	0.3112	1.50	1746 ± 23	1741 ± 31

Errors are 1σ; f_{206} is the percentage of common ^{206}Pb in total ^{206}Pb; Common Pb corrected using the measured ^{204}Pb.
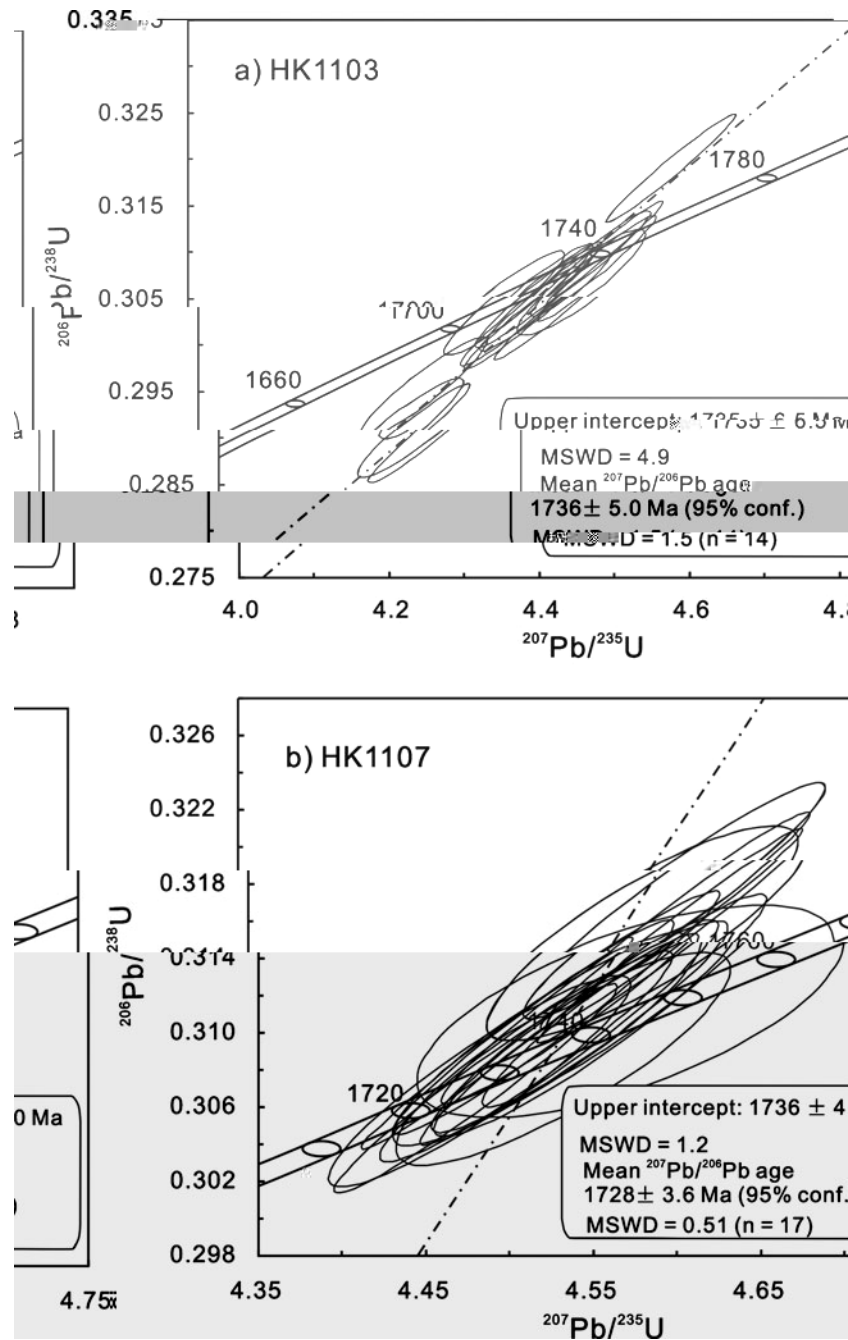
Figure 4. SIMS U–Pb Concordia diagrams of (a) sample HK1003 from the CZ; and (b) sample HK1007 from the OZ of the gabbroic rocks from the Hekou intrusion.

on CL images, and are 50–200 μm long with a length to width ratio of between 1:1 and 2:1 (Fig. 3b). Seventeen Cameca SIMS analyses were completed on 17 zircons with U concentration between 302 and 1533 ppm, Th between 388 and 2527 ppm, and Th/U ratios between 0.96 and 1.75 (Table 1). Most analyses yielded near concordant ages, while three grains are obviously discordant owing to the loss of radiogenic lead. All 17 analyses give consistent $^{207}Pb/^{206}Pb$ ratios within errors, yielding a weighted average $^{207}Pb/^{206}Pb$ age of 1728 ± 3.6 Ma (95 % confidence interval, MSWD = 0.51). In addition, all these 17 analyses yield a discordia line with an upper intercept age of 1736 ± 4.0 Ma (MSWD = 1.2) (Fig. 4b).

Combining the dating results above, the upper intercept ages for sample HK1103 and sample HK1107 are 1735 ± 6.5 Ma and 1736 ± 4.0 Ma, respectively. Therefore, the upper intercept ages of . 1736 Ma for the samples HK1103 and HK1107 are considered as the best estimate of the crystallization age for the gabbroic intrusion.

4.b. Elemental geochemistry

4. .1.   t   t   ff   t   t

All the samples analysed in this study were the freshest available based on outcrop appearances, but they were
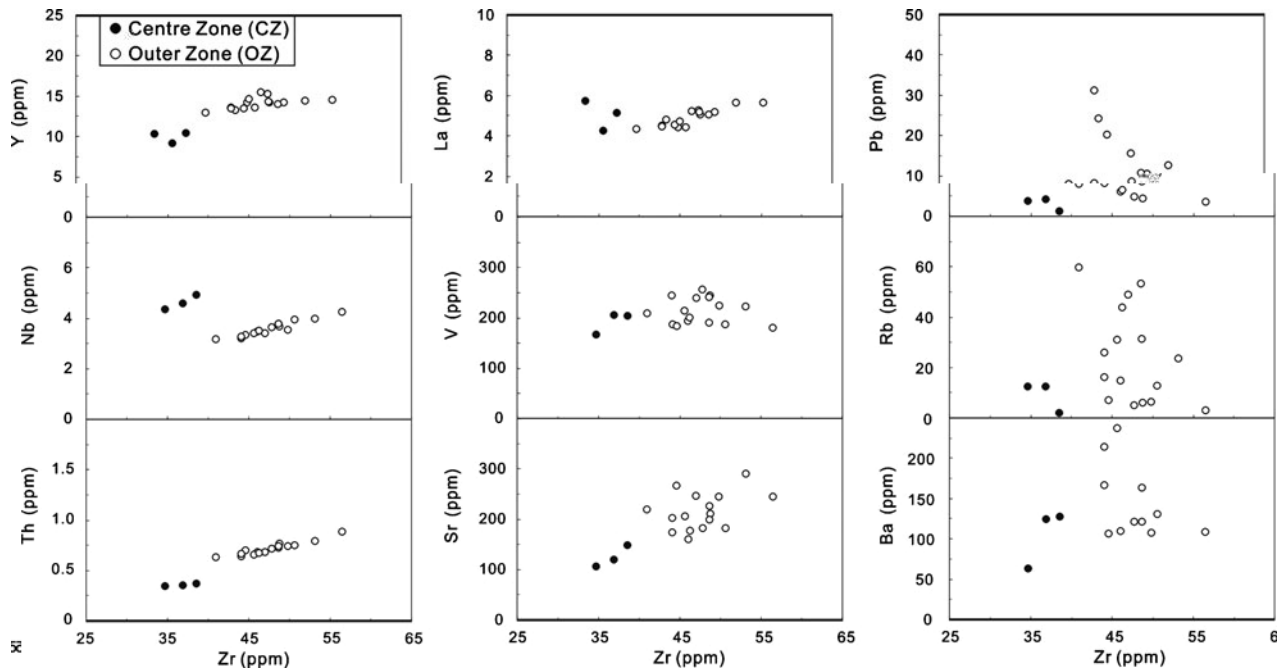
Figure 5. Diagrams of Y, Nb, Th, La, V, Sr, Pb, Rb and Ba v. Zr to evaluate the mobility of these elements in the gabbroic rocks from the Hekou intrusion during alteration. Solid round symbols – the central zone (CZ) of the gabbroic intrusion; Open round symbols – the outer zone (OZ) of the gabbroic intrusion.

altered to varying degrees judging from thin-section examinations. Nineteen samples from the Hekou gabbroic intrusion have been selected for major- and trace-element analyses (Table 2). The loss of ignition (LOI) values for the gabbroic rocks range from 0.55 to 2.69 %. Thus, the effects of alteration on the chemical compositions of these rocks need to be evaluated. Zirconium in mafic intrusive rocks is generally considered to be the most immobile during low- to medium-grade alteration (e.g. Wood, Joron & Treuil, 1979; Gibson *t* . 1982). Therefore, bivariate plots of Zr against selected trace elements have been used for evaluating the motilities of such elements during alteration (e.g. Polat, Hofmann & Rosing, 2002). A number of elements with different geochemical behaviours, including Y, Nb, Th, La, V, Sr, Rb, Rb and Ba in the gabbroic rocks, are plotted against Zr to evaluate their mobility during alteration. Except for Pb, Rb and Ba, the other elements overall correlated tightly with Zr, indicating that these elements are essentially immobile during alteration (Fig. 5). Therefore, only the immobile elements are used for geochemical classification and petrogenetic discussions in this study. Meanwhile, the sums of major-element oxides for all samples in this study are recalculated to 100 % volatile free.

4. .2.   - t - t   t

The rocks in the CZ of the Hekou gabbroic intrusion show fairly homogeneous major- and trace-element compositions, with Mg no. from 61.5 to 62.3, SiO_2 from 48.2 to 49.0 %, TiO_2 from 0.81 to 0.92 %, MgO ~8.9 %, Fe_2O_3 from 10.7 to 11.0 %, CaO 10.1 to 11.2 %, Al_2O_3 from 15.9 to 16.7 %, Zr from 34.7

to 38.5 ppm, Cr from 312 to 321 ppm, and Ni from 141 to 171 ppm (Table 2; Fig. 6). In contrast, the rocks from the OZ display slightly evolved compositions, with relatively lower Mg no. (54.3–59.3), MgO (6.9–8.4 %), Al_2O_3 (14.1–16.4 %), Cr (203–356 ppm) and Ni (74.6–113 ppm) contents, and higher SiO_2 (48.7–50.3 %), CaO (10.4–13.2 %) and Zr (40.9–56.5 ppm) concentrations than those of the rocks from the CZ of the intrusion. Meanwhile, TiO_2 (0.75–0.92 %) and Fe_2O_3 (48.7–50.3 %) contents of these rocks are similar to those of the rocks from the CZ (Table 2; Fig. 6). In the Fenner diagrams (Fig. 6), with decreasing MgO contents, Cr and Ni contents of the rocks from the OZ obviously decrease, and Fe_2O_3 contents slightly decrease, whereas SiO_2, TiO_2, CaO and Al_2O_3 contents slightly increase, and Zr contents obviously increase with decreasing MgO contents (Fig. 6). The Ti/Y ratios of the gabbroic rocks are 467–550 and 325–399 for the CZ and OZ, respectively. On the TAS rock classification diagram, all the gabbroic rocks from the intrusion are plotted in the subalkaline field (Fig. 7). Therefore, the gabbroic rocks from the Hekou intrusion were related to subalkaline basaltic affinities.

The gabbroic rocks from the Hekou intrusion have low total REE contents (REE = 29.3–40.2 ppm) (Fig. 8a). These rocks in the CZ of the intrusion show slightly LREE-enriched and HREE-depleted patterns (La_N = 14–18, $(La/Yb)_N$ = 3.1–4.0, $(La/Sm)_N$ = 1.8–1.9, $(Gd/Yb)_N$ = 1.4–1.7; subscript N denotes chondrite normalized) (Boynton, 1984), and slightly positive Eu anomalies (Eu/Eu^* = 1.2–1.3) (Fig. 8a). Compared with the rocks from the CZ of the intrusion, the OZ rocks have relatively flatter LREE and HREE patterns, with La_N = 14–18, $(La/Yb)_N$ = 2.1–2.7,

Table 2. Major-element (in wt %) and trace-element (in ppm) data for the gabbroic rocks from the Hekou intrusion

Rock type Sample no.	Gabbro HK1101	Gabbro HK1102	Gabbro HK1103	Gabbro HK1104	Gabbro HK1105	Gabbro HK1106	Gabbro HK1107	Gabbro HK1108
SiO_2	47.55	47.41	48.03	49.10	49.14	48.08	49.27	48.57
TiO_2	0.79	0.83	0.90	0.84	0.86	0.81	0.86	0.88
Al_2O_3	15.64	15.84	16.39	14.11	14.25	14.42	14.79	15.34
Fe_2O_3	10.46	10.81	10.55	11.21	10.68	11.31	11.06	10.57
MnO	0.09	0.10	0.12	0.22	0.20	0.20	0.19	0.21
MgO	8.73	8.70	8.71	7.50	7.64	7.77	7.38	7.00
CaO	11.03	10.84	9.85	11.67	12.62	12.56	12.84	12.56
Na_2O	3.41	3.29	3.21	2.26	2.98	2.23	1.93	2.47
K_2O	0.37	0.41	0.12	1.08	0.28	0.50	0.35	0.62
P_2O_5	0.04	0.06	0.06	0.07	0.07	0.06	0.07	0.06
LOI	1.27	1.08	1.46	1.23	0.66	1.32	0.55	1.11
Total	99.39	99.37	99.40	99.28	99.36	99.26	99.29	99.39
Mg no.	62.3	61.5	62.0	57.0	58.6	57.6	56.9	56.8
Sc	27.7	28.2	27.3	39.8	38.1	39.3	38.6	38.2
V	168	207	203	190	245	187	195	214
Cr	312	318	321	306	355	303	280	256
Co	46.8	54.8	52.9	46.2	43.8	52.4	47.7	46.9
Ni	160	171	141	100	97.6	113	100	95.5
Cu	29.7	26.4	34.4	109	70.1	109	99.4	105
Zn	29.2	39.8	46.7	129	80.0	149	104	112
Ga	14.2	14.8	15.4	14.8	14.5	14.8	14.5	15.2
Rb	12.6	12.6	2.00	53.4	5.96	26.1	14.8	30.9
Sr	107	120	149	226	210	174	161	206
Y	10.4	9.2	10.4	15.3	14.3	13.6	14.2	13.5
Zr	34.7	36.9	38.5	48.6	48.7	44.1	46.0	45.6
Nb	4.34	4.61	4.92	3.78	3.68	3.19	3.47	3.41
Cs	0.315	0.145	0.060	0.409	0.061	2.10	0.308	0.396
Ba	63.1	124	128	449	122	167	109	238
La	5.72	4.27	5.15	5.28	5.05	4.52	4.42	4.56
Ce	12.6	9.5	11.5	11.9	11.6	10.4	10.3	10.5
Pr	1.76	1.33	1.62	1.71	1.64	1.47	1.49	1.52
Nd	7.43	5.77	6.85	7.54	7.33	6.54	6.70	6.66
Sm	1.92	1.52	1.79	2.17	2.07	1.92	2.03	1.93
Eu	0.768	0.645	0.725	0.986	0.821	0.770	0.756	0.795
Gd	2.05	1.62	1.94	2.46	2.21	2.04	2.11	2.12
Tb	0.363	0.296	0.347	0.456	0.434	0.407	0.409	0.399
Dy	2.06	1.75	2.03	2.67	2.51	2.48	2.48	2.43
Ho	0.449	0.384	0.432	0.635	0.591	0.564	0.586	0.552
Er	1.13	0.99	1.15	1.66	1.56	1.52	1.51	1.44
Tm	0.151	0.143	0.160	0.236	0.212	0.207	0.224	0.215
Yb	0.960	0.939	1.08	1.50	1.43	1.38	1.43	1.36
Lu	0.133	0.145	0.159	0.239	0.215	0.207	0.210	0.202
Hf	1.07	1.09	1.23	1.56	1.59	1.37	1.40	1.36
Ta	0.297	0.299	0.312	0.246	0.243	0.217	0.232	0.221
Pb	3.85	4.14	1.29	15.7	4.50	31.2	6.03	20.3
Th	0.343	0.356	0.370	0.723	0.769	0.645	0.681	0.655
U	0.217	0.180	0.193	0.167	0.170	0.150	0.150	0.165

Table 2. Continued.

Rock type Sample no.	Gabbro HK1201	Gabbro HK1202	Gabbro HK1203	Gabbro HK1204	Gabbro HK1205	Gabbro HK1206	Gabbro HK1207	Gabbro HK1208	Gabbro HK1209	Gabbro HK1210	Gabbro HK1211
SiO_2	48.78	48.88	48.45	48.26	48.81	48.94	48.75	48.71	48.35	48.68	47.57
TiO_2	0.83	0.86	0.73	0.74	0.81	0.90	0.80	0.84	0.79	0.87	0.87
Al_2O_3	15.39	15.83	15.80	15.77	16.04	14.64	14.69	15.54	14.93	13.75	14.42
Fe_2O_3	10.51	10.34	9.95	10.38	9.85	11.44	10.76	10.25	10.83	11.43	11.19
MnO	0.21	0.18	0.21	0.20	0.21	0.21	0.22	0.20	0.26	0.19	0.21
MgO	7.54	6.84	7.20	7.17	6.80	6.85	7.91	7.31	7.81	8.19	8.18
CaO	10.09	13.05	12.02	11.69	12.33	12.76	12.39	12.01	11.58	11.92	12.90
Na_2O	2.77	2.20	2.69	2.83	2.37	1.58	1.84	2.30	2.42	1.90	2.05
K_2O	0.87	0.31	0.19	0.17	0.39	0.19	0.30	0.54	0.78	0.87	0.23
P_2O_5	0.05	0.07	0.06	0.06	0.07	0.07	0.06	0.07	0.06	0.06	0.07
LOI	2.69	1.19	2.32	2.09	2.12	2.18	1.85	1.59	1.79	1.52	2.12
Total	99.73	99.75	99.62	99.36	99.80	99.76	99.57	99.36	99.60	99.38	99.81
Mg no.	58.7	56.7	58.9	57.8	57.8	54.3	59.3	58.5	58.8	58.7	59.1
Sc	38.7	36.9	35.3	36.1	33.7	37.0	37.9	37.0	37.5	40.7	39.2
V	209	187	183	224	224	180	244	241	240	201	256
Cr	265	228	231	218	203	255	270	270	278	356	355
Co	48.7	46.3	38.6	40.1	38.8	42.1	47.0	47.1	47.9	52.0	42.8
Ni	99.2	88.2	78.3	75.6	74.6	80.1	91.0	89.8	92.5	101.4	91.9
Cu	108	93.3	108	116	83.0	83.7	110	102	98.9	94.2	72.1
Zn	97.0	106	248	374	127	86.5	135	150	214	104	94.6
Ga	13.8	15.8	15.0	15.0	15.5	16.9	13.7	15.3	14.7	14.3	14.6
Rb	59.7	12.8	6.96	6.27	23.5	2.94	16.1	31.4	48.8	43.8	4.92
Sr	219	181	266	244	290	245	203	199	246	177	183
Y	13.0	14.3	13.3	14.0	14.5	14.6	13.5	14.3	13.7	14.6	15.5
Zr	40.9	50.6	44.6	49.8	53.1	56.5	44.1	48.7	47.0	46.2	47.8
Nb	3.17	3.95	3.35	3.54	3.99	4.26	3.26	3.79	3.42	3.53	3.65
Cs	0.396	0.336	0.050	0.046	0.184	0.088	0.141	0.387	0.705	0.324	0.025
Ba	277	131	106	108	329	109	214	163	494	264	121
La	4.34	5.20	4.83	5.04	5.63	5.67	4.45	5.18	4.44	4.73	5.24
Ce	10.0	11.9	11.1	11.5	12.7	12.6	10.3	11.8	10.4	10.7	11.6
Pr	1.40	1.68	1.56	1.61	1.75	1.71	1.45	1.65	1.50	1.56	1.68
Nd	6.19	7.40	6.74	7.14	7.74	7.67	6.44	7.32	6.80	6.94	7.75
Sm	1.74	2.13	1.87	2.04	2.12	2.13	1.86	2.09	1.94	2.06	2.13
Eu	0.774	0.833	0.804	0.843	0.910	0.930	0.739	0.798	0.906	0.846	0.808
Gd	2.08	2.21	2.17	2.23	2.28	2.33	2.04	2.17	2.20	2.23	2.39
Tb	0.384	0.431	0.402	0.428	0.436	0.435	0.401	0.419	0.405	0.436	0.443
Dy	2.33	2.59	2.38	2.49	2.54	2.61	2.45	2.53	2.49	2.65	2.75
Ho	0.529	0.587	0.550	0.584	0.576	0.598	0.559	0.596	0.569	0.593	0.624
Er	1.40	1.52	1.44	1.48	1.52	1.58	1.44	1.54	1.51	1.58	1.60
Tm	0.206	0.224	0.200	0.210	0.217	0.226	0.219	0.201	0.215	0.226	0.233
Yb	1.28	1.42	1.34	1.42	1.41	1.49	1.28	1.42	1.39	1.49	1.50
Lu	0.192	0.222	0.188	0.202	0.202	0.211	0.217	0.199	0.201	0.218	0.222
Hf	1.27	1.51	1.39	1.58	1.56	1.72	1.38	1.51	1.45	1.44	1.49
Ta	0.195	0.255	0.215	0.230	0.339	0.269	0.217	0.237	0.217	0.223	0.233
Pb	8.00	10.5	24.2	10.8	12.7	3.49	8.13	8.59	54.7	6.45	4.93
Th	0.635	0.753	0.698	0.743	0.794	0.886	0.669	0.746	0.684	0.676	0.716
U	0.147	0.168	0.156	0.177	0.185	0.180	0.141	0.175	0.160	0.153	0.171

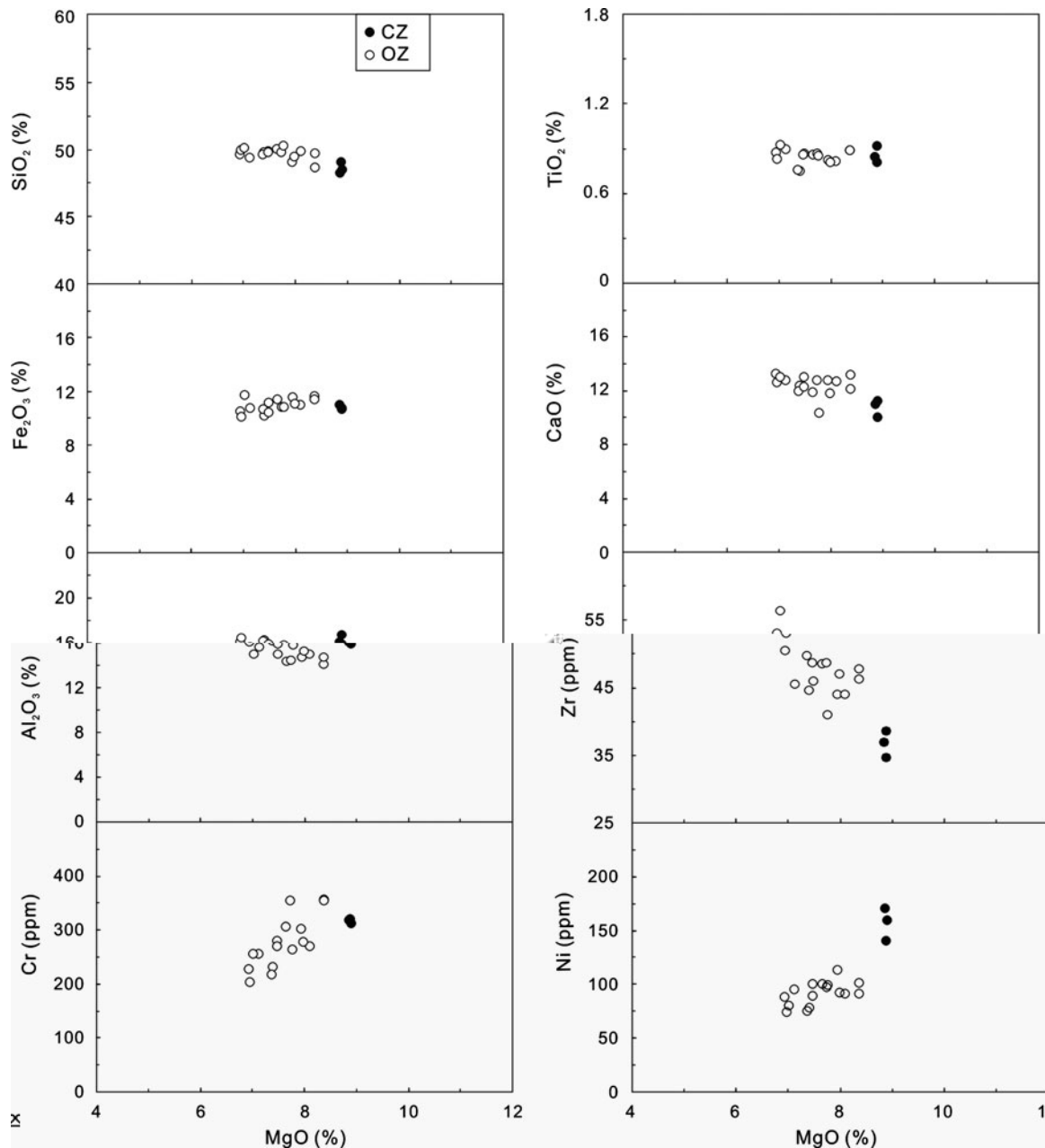Mg no. $=100*$ molar MgO/(Mg+FeO), assuming $FeO_T = 0.9 \times Fe_2O_3$. Total iron as FeO_T. LOI = loss on ignition.

Figure 6. Fenner diagrams for the gabbroic rocks from the Hekou intrusion. Symbols as in Figure 5.

$(La/Sm)_N = 1.4–1.7$, $(Gd/Yb)_N = 1.2–1.3$, and insignificant to slightly positive Eu anomalies ($Eu/Eu^* = 1.1–1.3$) (Fig. 8a).

In the primitive-mantle normalized multi-element plot (Sun & McDonough, 1989), the Hekou gabbroic rocks are characterized by the sub-parallel spiky pattern with slight enrichment in LREEs and large ion lithophile elements (LILEs), and slight depletion in HREEs and high field strength elements (HFSEs) (Fig. 8b). Notably, as shown in Figure 8b, these rocks from the CZ exhibit significant Th depletion (($Th/La)_{PM} = 0.49–0.67$; subscript PM denotes primitive-mantle normalized) and insignificant Nb and Ta depletion relative to La (($Nb/La)_{PM} = 0.73–1.0$, $(Ta/La)_{PM} = 0.87–1.2$). Meanwhile, the features of the CZ rocks are similar to E-MORB-like basaltic rocks, continental flood basalt (CFB) and ocean is-

land basalt (OIB) (Fig. 8b; Sun & McDonough, 1989). In contrast, these OZ rocks are slightly enriched in Th (($Th/La)_{PM} = 1.1–1.3$) and depleted in Nb and Ta (($Nb/La)_{PM} = 0.67–0.76$, $(Ta/La)_{PM} = 0.75–1.0$) (Fig. 8b).

4.c. Nd isotopes

Neodymium isotopic data are given in Table 3 for the Hekou gabbroic intrusion, of which the rocks from CZ and OZ have $^{147}Sm/^{144}Nd$ values of 0.1559–0.1590 and 0.1678–0.1772, and $^{143}Nd/^{144}Nd$ values of 0.512208–0.512327 and 0.512321–0.512400, corresponding to $\varepsilon_{Nd}(T)$ values of +0.70 to +2.3 and −0.30 to +0.24, respectively. The Nd isotopic compositions suggest that the parental magmas of the Hekou gabbroic intrusion were derived from a slightly depleted mantle source.

Table 3. Sm–Nd isotopic compositions for the gabbroic rocks from the Hekou intrusion

Sample	Sm (ppm)	Nd (ppm)	$^{147}Sm/^{144}Nd$	$^{143}Nd/^{144}Nd$ (2σ)	$(^{143}Nd/^{144}Nd)_I$	$\varepsilon_{Nd}(T)$
HK1101	1.916	7.430	0.1559	0.512208 (9)	0.510428	0.70
HK1102	1.517	5.769	0.1590	0.512327 (17)	0.510511	2.33
HK1103	1.794	6.850	0.1583	0.512273 (16)	0.510466	1.45
HK1106	1.917	6.538	0.1772	0.512400 (20)	0.510377	− 0.30
HK1206	2.128	7.667	0.1678	0.512321 (20)	0.510404	0.24
HK1207	1.856	6.443	0.1741	0.512386 (18)	0.510398	0.12

Chondrite uniform reservoir (CHUR) values ($^{147}Sm/^{144}Nd$ = 0.1967, $^{143}Nd/^{144}Nd$ = 0.512638) are used for the calculation. $\lambda_{Sm} = 6.54 \times 10^{-12}$ year^{-1} (Lugmair & Harti, 1978). The $(^{143}Nd/^{144}Nd)_I$ and $\varepsilon_{Nd}(T)$ of these rocks were calculated using the age of 1736 Ma.
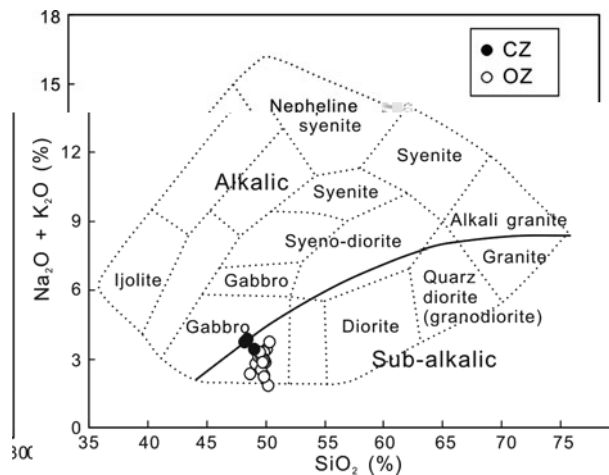
Figure 7. Rock classification plot of SiO_2 v. ($Na_2O + K_2O$) (Cox, Bell & Pankhurst, 1979) for the gabbroic rocks from the Hekou intrusion. Symbols as in Figure 5.

5. Discussion

5.a. The petrogenesis of the gabbroic intrusion

5. .1. *t t t*

The rocks from the CZ of the Hekou gabbroic intrusion show fairly homogeneous major oxides and Mg no. values. In contrast, the gabbroic rocks from the OZ of the intrusion exhibit slightly variable MgO concentrations and Mg no. values, suggesting that they had undergone small degrees of fractional crystallization (Fig. 6). A slight increase of TiO_2 with decreasing MgO contents for these rocks from the OZ indicates that TiO_2 was incompatible in the crystallizing phases and therefore titanomagnetite did not appear on the liquidus during crystallization of plagioclase and clinopyroxene in these systems. The slightly positive correlations of Fe_2O_3 versus MgO, and the obviously positive correlations of Cr and Ni versus MgO imply that they may undergo some degrees of fractionation of orthopyroxene.

The negative correlation of Al_2O_3 v. MgO in the rocks from the OZ suggests that they underwent insignificant plagioclase fractionation (Fig. 6; Pik *t* . 1998). The gabbroic rocks from the Hekou intrusion have relatively high CaO contents (10.1–13.2 %) and low REE contents (29.3–40.2 ppm), which are consistent with the features of the mafic cumulate rocks.

Moreover, all the rocks from the intrusion display a slightly negative correlation in the CaO v. MgO diagram (Fig. 6), implying clinopyroxene is a major fractionated phase for these rocks.

In summary, clinopyroxene and minor amounts of orthopyroxene are the important fractionation phases for the rocks from the OZ of the gabbroic intrusion.

5. .2. *C t t t*

The gabbroic rocks from the CZ of the intrusion display significant Th depletion and insignificant Nb and Ta depletion relative to La. In contrast, the gabbroic rocks in the OZ are slightly enriched in Th and depleted in Nb and Ta (Fig. 8b). As shown in the $\varepsilon_{Nd}(T)$–Nb/La plot (Fig. 9a; Paces & Bell, 1989) and the Nb/Th–Nb/La plot (Fig. 9b), the less-contaminated rocks from the CZ have relatively higher $\varepsilon_{Nd}(T)$ values and Nb–Ta contents, and lower Th contents than those of the more contaminated rocks from the OZ. In view of these geochemical and isotopic correlations, the crustal contaminants must mainly have caused low $\varepsilon_{Nd}(T)$ values, and Nb/La and Nb/Th ratios, indicating sialic crust components in the OZ rocks. Furthermore, the continental crust is typically depleted in Nb and Ta (Rudnick & Fountain, 1995), and the upper continental crust is enriched in La and Th while the lower continental crust is not usually enriched in Th (Barth, McDonough & Rudnick, 2000). As a result, the crustal contaminant, which is enriched in Th and La, and depleted in Nb and Ta, was potentially derived from the upper crust rather than from the lower crust (Fig. 9c; Ingle *t* . 2002). It is therefore suggested that the magmas parental to the gabbroic rocks assimilated the upper continental crust.

5. .3. *t f t t t t t*

Although the magmas parental to the Hekou gabbroic intrusion were subjected to variable degrees of crustal contamination, the rocks from the CZ exhibit obvious Th depletion and insignificant Nb, Ta and Ti depletions relative to La (Fig. 8b). However, the trace elemental features of the gabbroic rocks are different from those of typical E-MORB because: (1) all the gabbroic rocks are cumulate rocks and exhibit more obvious LREE-enriched and HREE-depleted patterns (Fig. 8a, b); (2)
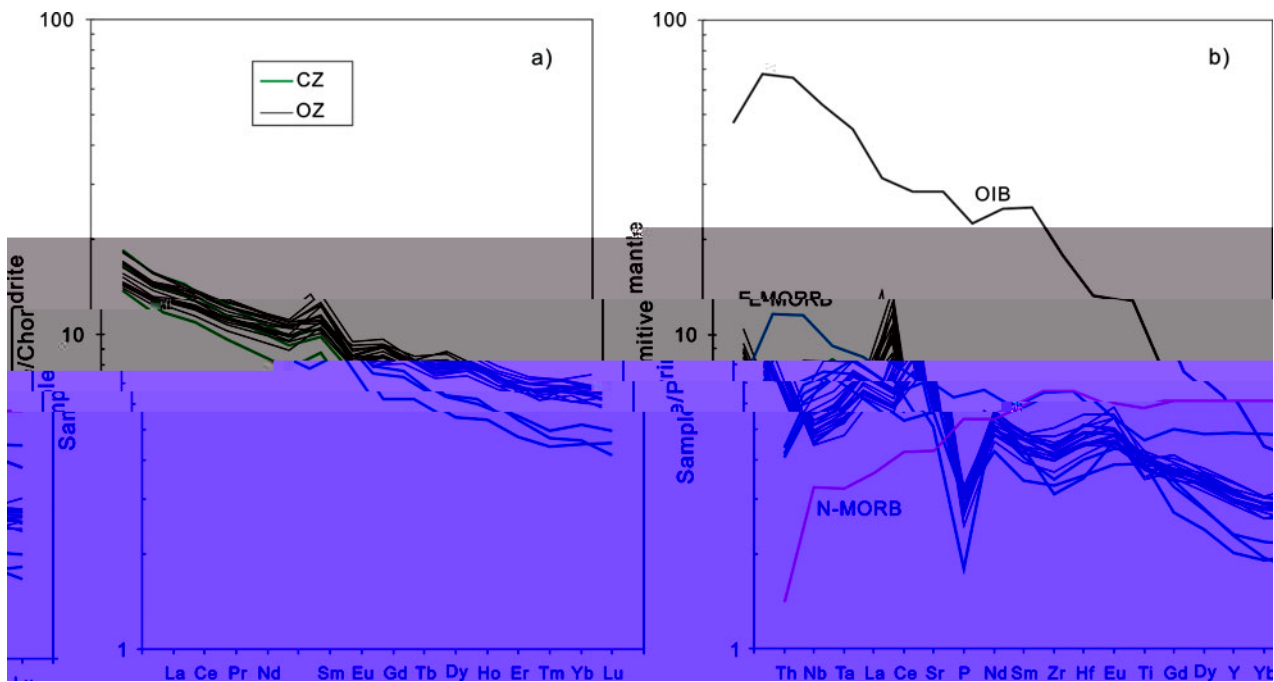
Figure 8. (Colour online) (a) Chondrite-normalized REE patterns; and (b) primitive-mantle normalized incompatible trace-element multi-element plot for the gabbroic rocks from the Hekou intrusion. The normalization values of chondrite are from Boynton (1984). The normalization values of primitive mantle are from Sun & McDonough (1989). Symbols as in Figure 5. OIB – ocean island basalt; E-MORB – enriched mid-ocean ridge basalt; N-MORB – normal mid-ocean ridge basalt.

the magmas parental to the gabbroic rocks had been assimilated by sialic crust. This makes it unlikely that the gabbroic intrusion was formed in an oceanic setting where sialic crust is normally absent. In contrast, the trace elemental features of the less-contaminated gabbroic samples are very similar to the intraplate basaltic rocks in CFB and OIB provinces (Sun & McDonough, 1989). For example, the less-contaminated rocks of the CZ have high Ti/Y (467–550) and low La/Nb (0.93–1.32) and La/Ta ratios (14.3–19.3), which are also similar to those of OIB (Ti/Y > 410, La/Nb < 1.5 and La/Ta < 22) (Table 2; Ormerod *t* . 1988; Sun & McDonough, 1989; Lightfoot *t* . 1993; Garland, Turne & Hawkesworth, 1996; Ewart *t* . 1998).

Based on the aforementioned results, the magmas parental to the gabbroic rocks display a subalkaline basaltic affinity. In combination with the Nd isotopic features ($\varepsilon_{Nd}(T) = +0.70$ to $+2.3$) of the less-contaminated rocks from the CZ, the parental magmas for the Hekou gabbroic rocks were proposed to be generated dominantly by melting of a slightly depleted mantle source. The lack of Nb–Ta depletion and the high-Ti nature of the magma parental to the less-contaminated rocks suggest the sub-continental lithospheric mantle (SCLM) was not the geological reservoir that contributed the trace-element and Nd isotope inventory to the Hekou gabbroic intrusion. In general, low ratios of LREE/HREE in mafic rocks reflect a melting regime dominated by relatively large melting fractions and/or having spinel as the predominant residual phase, whereas high LREE/HREE ratios are indicative of smaller melting fractions and/or garnet control

(Deniel, 1998; Xu *t* . 2001). Therefore, the samples from the Hekou gabbroic intrusion, exhibiting a slightly LREE-enriched and HREE-depleted pattern, were potentially generated by relatively high degrees of partial melting of a slightly depleted asthenospheric mantle source. Their geochemical and isotopic variations are attributed to slight crystal fractionation with varying degrees of crustal contamination.

5.b. Tectonic implications

Numerous meta-volcanic- and meta-sedimentary-rock-hosted Fe–Cu ore deposits were developed in the late Palaeoproterozoic to early Mesoproterozoic basins in the Kangdian region in the southwestern Yangtze Block, for example, the Dahongshan, Hekou, and Dongchuan Fe–Cu ore deposits (D. F. He, unpub. Ph.D. thesis, Graduate School of the Chinese Academy of Sciences, 2009; Zhao *t* . 2010, 2013; Zhao & Zhou, 2011; Chen & Zhou, 2012). The ages of the meta-volcanic rocks and mafic intrusions from the upper Palaeoproterozoic to lower Mesoproterozoic strata in the Kangdian region had recently been well constrained by the availability of precise U–Pb zircon ages (Greentree & Li, 2008; D. F. He, unpub. Ph.D. thesis, Graduate School of the Chinese Academy of Sciences, 2009; Zhao *t* . 2010, 2013; Zhao & Zhou, 2011; Chen, Zhou & Zhao, 2013). However, such meta-volcanic rocks and mafic intrusions (Greentree & Li, 2008; D. F. He, unpub. Ph.D. thesis, Graduate School of the Chinese Academy of Sciences, 2009; Zhao *t* . 2010, 2013; Zhao & Zhou, 2011; Chen, Zhou & Zhao, 2013)
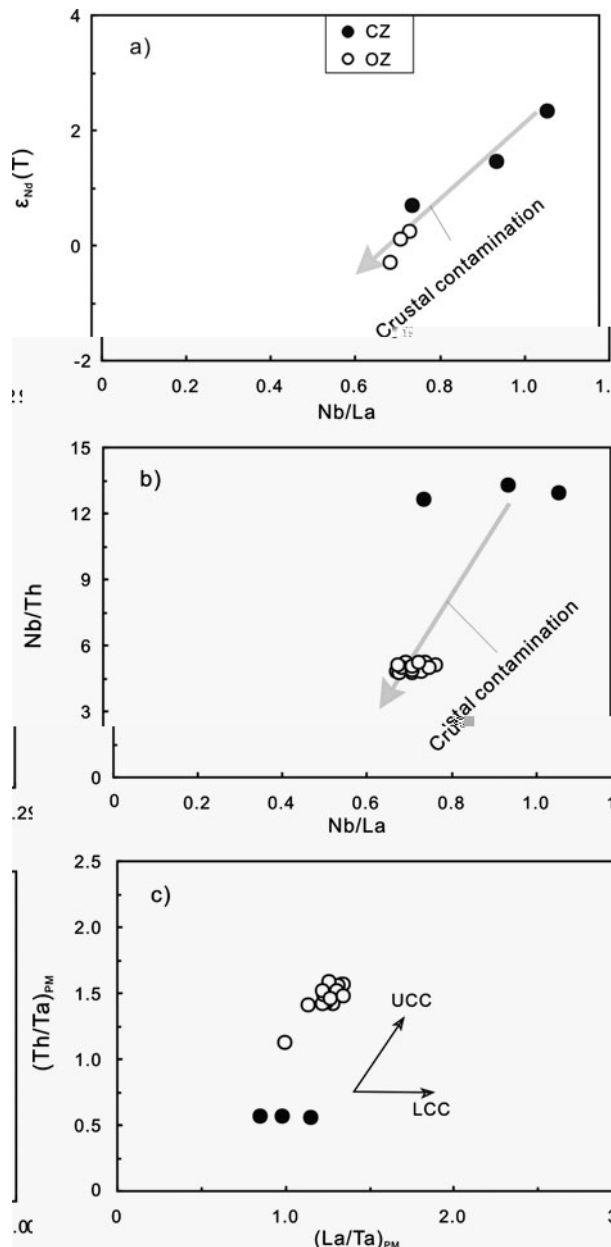
Figure 9. Plots of (a) $\varepsilon_{Nd}(T)$ v. Nb/La; (b) Nb/Th v. Nb/La; and (c) $(Th/Ta)_{PM}$ v. $(La/Ta)_{PM}$ (Ingle *et al.* 2002) for the gabbroic rocks from the Hekou intrusion. Symbols as in Figure 5. UCC – upper continental crust; LCC – lower continental crust.
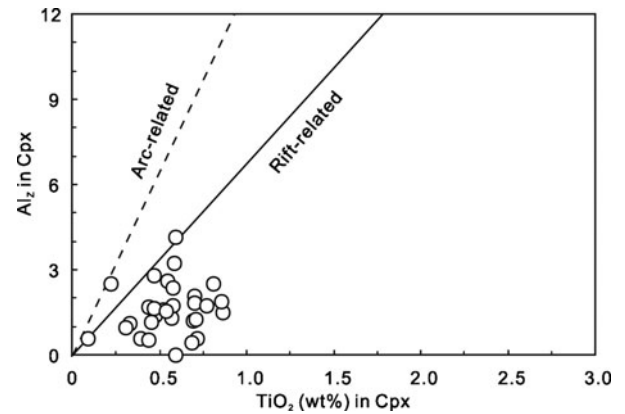

Figure 10. Discrimination diagram of Al_Z (percentage of tetrahedral sites occupied by Al) v. TiO_2 in clinopyroxenes (Loucks, 1990) for the gabbroic rocks from the Hekou intrusion. Symbols as in Figure 5.

were generally intensely altered and did not preserve their original chemical characteristics. Therefore, a major problem with better understanding these deposits is the lack of precise elemental and isotopic data for these meta-volcanic rocks and mafic intrusions, which hampers the understanding of the geodynamic setting of the ore mineralization.

The Hekou gabbroic intrusion has a SIMS U–Pb zircon age of *c.* 1736 Ma reported in this study, suggesting that the depositional ages of the Hekou Group were slightly older than the ages of the intrusion (Chen, Zhou & Zhao, 2013). Moreover, the crystallization ages of the gabbroic intrusion are similar to that of the dolerite dykes that intruded into the Dahongshan Group in the Dahongshan Fe–Cu ore deposit (Zhao & Zhou, 2011)

and into the Lower Kunyang Group in the Yinmin Fe–Cu ore deposit (Zhao *et al.* 2010, 2013), indicating that significant mafic magmatism occurred at *c.* 1.7 Ga in the southwestern Yangtze Block. The meta-volcanic rocks from the Dahongshan Group and the Yinmin Formation in the Lower Kunyang Group were also formed slightly before or almost synchronously with the *c.* 1.7 Ga mafic dykes and intrusions (Greentree & Li, 2008; D. F. He, unpub. Ph.D. thesis, Graduate School of the Chinese Academy of Sciences, 2009; Zhao & Zhou, 2011; Zhao *et al.* 2010, 2013). Therefore, the late Palaeoproterozoic to Mesoproterozoic volcanic and sedimentary basins, termed the Dahongshan, Hekou and Lower Kunyang groups, were likely formed almost synchronously and slightly prior to *c.* 1.7 Ga.

As discussed above, the least-contaminated gabbroic rocks from the CZ exhibit characteristic patterns of incompatible trace elements similar to those of OIB and CFB (Fig. 8b). As shown in Figure 10, the clinopyroxene crystals from the Hekou intrusion show the characteristics of gabbroic cumulate rocks formed in a continental rift system. Magmatism associated with lithosphere rifting coupled with asthenosphere upwelling can explain why the intrusion has isotopic compositions similar to those of magmas derived from the asthenospheric mantle. Therefore, the gabbroic intrusion intruded into the Hekou Group is best interpreted as a product of a continental rift environment.

In the Kangdian region, the Yinmin Formation of the Lower Kunyang Group with a U–Pb zircon age of 1742 ± 13 Ma has been considered to have formed in a continental rift basin (Hua, 1990; Wu *et al.* 1990; Zhao *et al.* 2010). Meanwhile, alkali basaltic tuff is present in the Yinmin Formation (Wu *et al.* 1990; Greentree *et al.* 2006). Moreover, the $\varepsilon_{Hf}(t)$ values of igneous zircons from the tuff and ~1.70 to 1.65 Ga dolerite dykes that intruded into the Yinmin Formation suggest they were derived from a depleted mantle source. These dolerite dykes show no anomalies of Nb and Ta on the

primitive-mantle normalized multi-element plot, and fall into the field of within-plate basalt (Zhao *t .* 2010, 2013; Zhao & Zhou, 2011). These sedimentary records combined with the elemental and isotopic data from these igneous rocks support the interpretation that the Yinmin Formation of the Lower Kunyang Group was formed in a continental rift setting at ∼1.7 Ga. It is therefore suggested that the . 1.7 Ga Dahongshan, Hekou and Lower Kunyang groups were likely formed in similar continental rift basins in the southwestern Yangtze Block.

Collisional events at 2.1 to 1.8 Ga have been recorded in a number of Precambrian cratons and are thought to be related to the assembly of the Palaeoproterozoic supercontinent Columbia (Rogers & Santosh, 2002; Zhao *t .* 2002). More recently, it was suggested that even the 1.84–1.75 Ga mafic dyke swarms and 1.75–1.68 Ga anorthosite–mangerite–alkali granite and rapakivi granite suites (AMGRS) in the North China Craton (NCC) may have resulted from the fragmentation of the Columbia supercontinent (e.g. Zhao *t .* 2002 ; Peng, Zhai & Guo, 2006; Peng *t .* 2007, 2008; Hou *t .* 2008 ,). The late Palaeoto Mesoproterozoic anorogenic magmatism associated with the break-up of the Columbia supercontinent generally took place during intraplate continental rifting, triggered mostly by mantle plumes (Rogers & Santosh, 2002; Zhao *t .* 2002 , 2004; Peng *t .* 2008; Hou *t .* 2008 , ; Evans & Mitchell, 2011).

In the traditional reconstruction models (Rogers & Santosh, 2002; Zhao *t .* 2002), the Yangtze Block was not included in the Columbia supercontinent owing to the lack of geological and geochronological data for that time. However, recent studies reveal that the Yangtze Block may have been involved in this global Palaeoproterozoic orogenic event (Zhang *t .* 2006 ; Sun *t .* 2008; Wu *t .* 2008; Peng *t .* 2009, 2012) and late Palaeo- to Mesoproterozoic anorogenic magmatism (Zhao *t .* 2010, 2013; Chen, Zhou & Zhao, 2013). In this study, the presence of the . 1.7 Ga Hekou gabbroic intrusion in the southwestern Yangtze Block is contemporaneous with the break-up of the Columbia supercontinent, which provides further evidence to support the idea that the Yangtze Block was likely a part of the supercontinent.

It is difficult to tell the precise position of the Yangtze Block within the Columbia supercontinent without a large number of reliable palaeomagnetic poles. However, on the basis of similar age spectra of detrital zircons, the geochemical characteristics of the Palaeoproterozoic strata, comparisons of rift-related sediments and ∼1.7 Ga within-plate mafic magmatism (such as the Hekou intrusion reported in this paper) among different blocks in the Columbia supercontinent, the Yangtze Block is considered to possibly link with the North Australian Craton during Palaeoproterozoic time (Wang *t .* 2012; Chen, Zhou & Zhao, 2013; Chen *t .* 2013; Chen, Zhang & Song, 2013; Wang & Zhou, 2014), as reconstructed by Zhao *t .* (2002 , 2004). Moreover, the Yangtze Block, the NW India and the North Australian Craton were perhaps neighbours located in a spatial association within the Columbia supercontinent, based on the similar mineralization ages and styles of the Palaeoproterozoic Fe–Cu ore deposits on these cratons (Zhou *t .* 2014).

6. Conclusions

(1) The age of crystallization for the Hekou gabbroic intrusion is ∼1.7 Ga, as demonstrated by the upper intercept ages of 1735 ± 6.5 Ma and 1736 ± 4.0 Ma for the rocks from the CZ and the OZ, respectively.

(2) The Hekou gabbroic intrusion experienced slight fractional crystallization from a parental magma, which was potentially generated by melting of a slightly depleted asthenospheric mantle source in a continental rift environment plus varying degrees of crustal contamination.

(3) The Yangtze Block was likely a fragment of the Palaeo- to Mesoproterozoic supercontinent Columbia, and the . 1.7 Ga Hekou gabbroic intrusion from the southwestern Yangtze Block was likely formed in an anorogenic continental rift that contributed to the break-up of the Columbia supercontinent.

Supplementary material

To view supplementary material for this article, please visit http://dx.doi.org/10.1017/S0016756815001119.

References

BARTH, M. G., MCDONOUGH, W. F. & RUDNICK, R. L. 2000. Tracking the budget of Nb and Ta in the continental crust. *C* **165**, 197–213.

BOYNTON, W. V. 1984. Geochemistry of the rare earth elements: meteorite studies. In *t t - t* (ed. P. Henderson), pp. 63–114. Amsterdam: Elsevier.

CHANG, X., ZHU, B., SUN, D., QIU, H. & ZOU, R. 1997. Isotope geochemistry study of Dongchuan copper deposits in Middle Yunnan Province, SW China: stratigraphic chronology and application of geochemical exploration by lead isotopes. **26**, 32–8 (in Chinese with English abstract).

CHEN, Z. C., LIN, W., FAURE, M., LEPVRIER, C., CHU, Y. & WANG, Q. C. 2013. Geochronological constraint of early Mesozoic tectonic event at Northeast Vietnam. *t t* **29**, 1825–40.

CHEN, L., ZHANG, Z. & SONG, H. 2013. Weak depth and along-strike variations in stretching from a

multi-episodic finite stretching model: evidence for uniform pure-shear extension in the opening of the South China Sea. *f* *t* **78**, 358–70.

CHEN, W. T. & ZHOU, M. F. 2012. Paragenesis, stable isotopes, and molybdenite Re–Os isotope age of the Lala iron–copper deposit, Southwest China. **107**, 459–80.

CHEN, W. T., ZHOU, M. F. & ZHAO, X. F. 2013. Late Paleoproterozoic sedimentary and mafic rocks in the Hekou area, SW China: implication for the reconstruction of the Yangtze Block in Columbia. **231**, 61–77.

CONG, B. L. (ed.) 1988. *t* *t* *f* - *ft*. Beijing: Science Press, 424 pp (in Chinese with English abstract).

COX, K. G., BELL, J. D. & PANKHURST, R. J. 1979. *t* - *t* *t* *f*. London: Allen and Unwin, 450 pp.

DENIEL, C. 1998. Geochemical and isotopic (Sr, Nd, Pb) evidence for plume-lithosphere interactions in the genesis of Grande Comore magmas (Indian Ocean). *C* **144**, 281–303.

EVANS, D. A. D. & MITCHELL, R. N. 2011. Assembly and breakup of the core of Paleoproterozoic–Mesoproterozoic supercontinent Nuna. **39**, 443–6.

EWART, A., MILNER, S. C., ARMSTRONG, R. A. & DUNCAN, A. R. 1998. Etendeka volcanism of the Goboboseb Mountains and Messum igneous complex, Namibia. Part I: geochemical evidence of early Cretaceous Tristan Plume melts and the role of crustal contamination in the Parana-Etendeka CFB. *f* *t* **39**, 191–225.

FAN, H. P., ZHU, W. G., LI, Z. X., ZHONG, H., BAI, Z. J., HE, D. F., CHEN, C. J. & CHAO, C. Y. 2013. Ca. 1.5 Ga mafic magmatism in South China during the break-up of the supercontinent Nuna/Columbia: the Zhuqing Fe–Ti–V oxide ore-bearing mafic intrusions in western Yangtze Block. *t* **168–169**, 85–98.

GAO, S., YANG, J., ZHOU, L., LI, M., HU, Z., GUO, J., YUAN, H., GONG, H., XIAO, G. & WEI, J. 2011. Age and growth of the Archean Kongling terrain, South China, with emphasis on 3.3 Ga granitoid gneisses. *f* **311**, 153–82.

GARLAND, F., TURNE, S. & HAWKESWORTH, C. 1996. Shifts in the source of the Paraná basalts through time. *t* **37**, 223–43.

GENG, Y., YANG, C., DU, L., WANG, X., REN, L. & ZHOU, X. 2007. Chronology and tectonic environment of the Tianbaoshan formation: new evidence from zircon SHRIMP U–Pb age and geochemistry. **53**, HEN

lithosphere by a mantle plume: major-, trace-element, and Sr-, Nd-, and Pb-isotope evidence from picritic and tholeiitic lavas of the Noril'sk District, Siberian Trap, Russia.*C*   *t*   *t*   *t*   *t*   **114**, 171–88.
Loucks

petrogenesis of Permian–Triassic Emeishan flood basalts in southwestern China. *t* **58**, 145–68.

YAO, J., SHU, L. & SANTOSH, M. 2011. Detrital zircon U–Pb geochronology, Hf-isotopes and geochemistry — new clues for the Precambrian crustal evolution of Cathaysia Block, South China. **20**, 553–67.

YIN, F. G., SUN, Z. M. & ZHANG, Z. 2011. Mesoproterozoic stratigraphic-structure framework in Huili-Dongchuan area. **57**, 770–8 (in Chinese with English abstract).

ZHANG, C. H., GAO, L. Z., WU, Z. J., SHI, X. Y., YAN, Q. R. & LI, D. J. 2007. SHRIMP U–Pb zircon age of tuff from the Kunyang group in central Yunnan: evidence for Grenvillian orogeny in south China. *C t* **52**, 1517–25.

ZHANG, S., LI, Z. X., EVANS, D. A. D., WU, H. & LI, H. 2012. Pre-Rodinia supercontinent Nuna shaping up: a global synthesis with new paleomagnetic results from North China. *t t tt* **353–354**, 145–55.

ZHANG, S. B., ZHENG, Y. F., WU, Y. B., ZHAO, Z. F., GAO, S. & WU, F. Y. 2006. Zircon isotope evidence for ≥ 3.5 Ga continental crust in the Yangtze craton of China. **146**, 16–34.

ZHANG, S. B., ZHENG, Y. F., WU, Y. B., ZHAO, Z. F., GAO, S. & WU, F. Y. 2006. Zircon U–Pb age and Hf–O isotope evidence for Paleoproterozoic metamorphic event in South China. **151**, 265–88.

ZHAO, G. C., CAWOOD, P. A., WILDE, S. A. & SUN, M. 2002. Review of global 2.1–1.8 Ga orogens: implications for a pre-Rodinia supercontinent. *t -* **59**, 125–62.

ZHAO, G. C., SUN, M., WILDE, S. A. & LI, S. Z. 2004. A Paleo-Mesoproterozoic supercontinent: assembly, growth and breakup. *t -* **67**, 91–123.

ZHAO, X. F. & ZHOU, M. F. 2011. Fe–Cu deposits in the Kangdian region, SW China: a Proterozoic IOCG (iron–oxide–copper–gold) metallogenic province. *t* **46**, 731–47.

ZHAO, X. F., ZHOU, M. F., LI, J. W., SUN, M., GAO, J. F., SUN, W. H. & YANG, J. H. 2010. Late Paleoproterozoic to early Mesoproterozoic Dongchuan Group in Yunnan, SW China: implications for tectonic evolution of the Yangtze Block. **182**, 57–69.

ZHAO, X. F., ZHOU, M. F., LI, J. W. & QI, L. 2013. Late Paleoproterozoic sedimentary rock-hosted stratiform copper deposits in South China: their possible link to the supercontinent cycle. *t* **48**, 129–36.

ZHAO, T. P., ZHOU, M. F., ZHAI, M. G. & XIA, B. 2002. Paleoproterozoic rift-related volcanism of the Xiong'er group, North China craton: implications for the breakup of Columbia. *t t* **44**, 336–51.

ZHENG, J. P., GRIFFIN, W. L., O'REILLY, S. Y., ZHANG, M., PEARSON, N. & PAN, Y. 2006. Widespread Archean basement beneath the Yangtze Craton. **34**, 417–20.

ZHOU, M. F., ZHAO, X. F., CHEN, W., LI, X. C., WANG, W., YAN, D. P. & QIU, H. N. 2014. Proterozoic Fe-Cu metallogeny and supercontinental cycles of the southwestern Yangtze Block, southern China and northern Vietnam. *t -* **139**, 59–82.

ZHOU, J. Y., ZHENG, R. C., ZHU, Z. M., CHEN, J. B., SHEN, B., LI, X. Y. & LUO, L. P. 2009. Geochemistry and Sm–Nd dating of the gabbro in the Lala copper ore district, Sichuan Province. China. *t f , t t* **28**, 111–22 (in Chinese with English abstract).